Engineering Science and Technology, an International Journal 24 (2021) 579–588

HOSTED BY

Contents lists available at ScienceDirect

Engineering Science and Technology, an International Journal

journal homepage: www.elsevier.com/locate/jestch

Full Length Article

Experimental investigation on deformation behavior and energy absorption capability of nested steel tubes under lateral loading

Yaşar Kahraman *, Ortaç Akdikmen

Faculty of Engineering, Mechanical Engineering Department, Sakarya University, Sakarya, Turkey

ARTICLE INFO

Article history:
Received 24 September 2020
Revised 30 December 2020
Accepted 4 January 2021
Available online 30 January 2021

Keywords:
Nested structure
Lateral loading
Steel tubes
Energy efficiency
Specific energy absorption

ABSTRACT

The energy absorption behavior of nested tubes under lateral loading conditions was investigated in this study. Nested tubes are considered as an alternative to energy absorption structures used in many industries including automotive, military, and aerospace. Steel tubes with the same wall thickness and different diameters were used in the experiments. First, experiments of single tubes were carried out, and the deformation behavior of tubes under lateral load was examined in detail. Afterward, experiments were carried out on nested tube samples in which a minimum of 2 and a maximum of 6 tubes were used together in different numbers and sequences. It was seen from the experiments that the best-nested tube configuration in terms of energy absorption capacity was the sample that contains 6 tubes with 1767 J. While this sample absorbed 5% higher energy than the sample with 5 tubes, the specific energy absorption value was calculated to be 10% lower. Additionally, the sample with 6 tubes has a value of 43% in terms of energy efficiency which is 7% lower compared to that of the sample with 5 tubes. It was determined that the sample with 5 tubes yielded the most efficient design when specific energy absorption capability, work effectiveness, and energy efficiency parameters were considered.

1. Introduction

Due to their efficient energy absorption capability, metallic tubes are preferred as energy absorption devices in many different applications such as vehicles, aircraft, and trains. During the last half-century, a significant number of studies on thin-walled tubes have been conducted. In these studies, thin-walled tubes with different cross-sections (circular, square, triangle, etc.) [1–3] and materials (steel, aluminum, composite, etc.) [4–6] were used. Additionally, different loading conditions such as quasi-static [7–9] and impact [10–12] loadings were studied as an important parameter. The studies also can be classified into two main groups according to the loading type of tubes as axially [13–18] and laterally [19–23].

The studies on axially loaded tubes have the greatest portion in the literature due to their higher energy absorption capacities compare to lateral loading. Although the axially loaded tubes offer some advantages, the large fluctuation in compressive force and different deformation modes (occurred related to the geometrical properties) are some of its drawbacks. In addition, the bending without folding and the off-axis loading are one of the main restrictions for these tubes as an unstable deformation mode. In contrast to axial loading, the force curve has an almost constant value for large displacement and there are no unstable deformation modes during the lateral compression of tubes [23].

There are many studies on deformation behavior and energy absorption capability of laterally compressed tubular structures between flat plates. In addition to experimental studies, there are some theoretical [24–26] and numerical [27,28] studies as well. Yella et al. [24] experimentally investigated the radial crushing behavior of tubes with restricted lateral movements. They reported that the energy absorbed by these tubes was three times greater than that of unrestrained tubes. Deruntz and Hodge [25] derived a formula for the compression force for short length circular tubes. Reid and Reddy [26] improve a theoretical model by considering the strain hardening effect. Gupta et al. [27] investigated experimentally and numerically the conditions of circular, triangular, and square tubes under radial loading. They reported that in samples with the same thickness, the deformation of the tube with a lower diameter occurred at higher forces, and the ability to absorb energy was higher in these tubes. They also found that square-section tubes with equal cross-sectional areas absorb higher energy than triangular cross-section ones. Alghamdi [29], who compiled the studies on tube structures with different cross-

* Corresponding author.
E-mail address: kahraman@sakarya.edu.tr (Y. Kahraman).
Peer review under responsibility of Karabuk University.

https://doi.org/10.1016/j.jestch.2021.01.002
2215-0986/

sectional areas, stated that the deformation behavior is more stable in radial loading than axial loading.

Because of obtaining low absorbed energy under lateral compression, tubes were filled with foam [30,31], or multi-tube configuration was used [32,33] in some studies to increase the absorbed energy. Olabi et al. [33] investigated the lateral crushing behavior of a multi-tube sample obtained by using three tubes with different diameters under quasi-static load, free and restricted from the sides. Yu et al. [34] proposed the use of a multi-tube sample consisting of three tubes that would absorb the explosion effect and analyzed this sample experimentally and numerically. They found that the proposed sample combination offers the most stable and efficient energy absorption value. They also demonstrated that the multi-tube adapted door design with a lower weight, developed in this study, dampens the explosion like its counterparts.

The literature on the performance of nested tubes that contain more than 3 tubes is quite limited. Hence, this study aimed to investigate the deformation behavior and energy absorption capability of nested tubes that contain a minimum of 2 and a maximum of 6 tubes. The nested tubes were fabricated by using the same wall thickness steel tubes of four different diameters. The samples were evaluated according to various criteria in terms of energy efficiency, and the most efficient design of the nested tube was determined.

2. Experimental study

2.1. Material properties and sample preparation

Four different diameters of seamless DIN S235JR steel tubes with the same wall thickness were used in the experimental study. The manufacturer gives the minimum yield strength as 235 MPa and the tensile strength of 360 MPa – 510 MPa for steel tubes. In order to determine the mechanical properties of the steel tubes, the tensile test was carried out according to the ASTM-E8/E8M – 09 standard for pipes with a diameter higher than 19 mm. As a result, the yield and tensile strengths were found to be 274 MPa and 465 MPa, respectively, and the elongation amount was 21%.

Steel tubes were obtained by machining from pipes of 95 mm, 45 mm, 38 mm, and 24 mm diameters, and approximately 10 mm wall thickness, respectively. With this process, it was ensured that the wall thicknesses were equal in the whole cross-section, and the scattering that may occur during the experiment repetitions was prevented. Steel tubes are coded as the largest diameter ST-1 and the smallest diameter ST-4 (single tube), and these tubes are used in nested tubes sample combinations. The schematic view of steel tubes is given in Fig. 1, and the geometric sizes of these tubes are given in Table 1. While determining the tube diameters, it was especially taken into consideration that two ST-2 tubes can be inserted into the ST-1 tube.

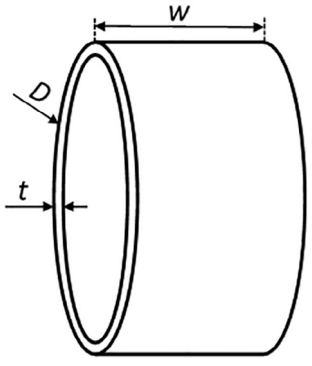

Fig. 1. Schematic view of steel tube used in experiments.

Table 1
Geometric sizes of the steel tubes.

Sample name	D (mm)	t (mm)	w (mm)
ST-1	90	2. 5	40
ST-2	42.5	2.5	40
ST-3	35	2.5	40
ST-4	20	2.5	40

Nested tube samples were obtained by using ST-1 - ST-4 tubes in different combinations. The tubes that are used to create the nested tube should be held in proper design before the loading and they should protect their alignment during the experiment as well. A special apparatus has been designed to ensure the position accuracy in the assembly of the tubes, which is important in case of obtaining identical samples (by means of alignment). The point welding was applied where the tubes are in touch (only on the upper surface side of the tubes) by using the electric arc welding method after they were placed on the apparatus. In Fig. 2, this special apparatus, two tubes in sequence before welding, and the ready-to-test sample (point welded) photos are given together.

In Fig. 3, pre-experiment images of nested tube samples are given. Samples are divided into groups according to the total number of tubes. The number in the sample names indicates the number of tubes in the sample, and the letter indicates the index in that group. Two main criteria were used to form the nested tube;

i- in all nested tube combinations (except NT2) the inner tubes were aligned as to whether they were in contact with the main tube or not.

ii- each ST tubes should be used at least once in each nested tube. However, this could not be applied due to the number of single tubes in NT2 and NT3 samples.

As can be seen in Fig. 3, at least two and at most six tubes were used in sample combinations. Since the NT2 sample was used to examine the deformation behavior of multiple tubes, only one sample combination was used in this group. In the NT6 group, again, only one combination was used, since a different combination could not be created in the sequence of the tubes. The numbers of ST-1/4 tubes in nested tubes and their weight are given in Table 2.

2.2. Experimental Set-up

The quasi-static tests of single and nested steel tube samples were carried out using a four-column hydraulic press with a capacity of 250 kN given in Fig. 4. The data of the force–displacement pair are recorded simultaneously with the experiments at a frequency of six data/s. In the experiments, the deformation rate was determined as 60 mm/min, and all experiments were recorded by using a camera.

3. Results

Experiments were repeated at least three times for each sample combination, but curves with mean values were used to avoid data complexity. The maximum displacement value for all samples was determined as 85% of the calculated crushing values. This situation is particularly preferred to prevent damages caused by excessive deformation in the tubes and to protect the test device from harm that may occur due to high force values. ST-1 tube has always been used as the main tube in forming nested tubes. Different combinations were obtained by placing other tubes in different numbers and/or different sequences in the ST-1.

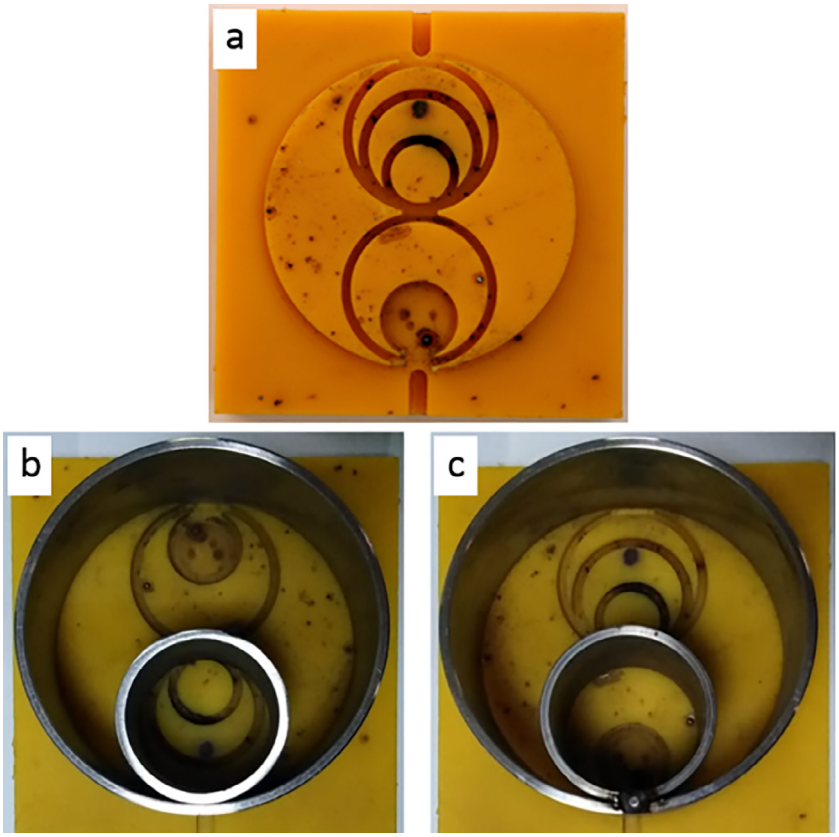

Fig. 2. The apparatus used in connecting the tubes and a sample tube (a) the apparatus used in the welding process, (b) the tube before welding, and (c) welded view of a nested tube.

3.1. Deformation of steel tubes under lateral loading

There are many studies in the literature on lateral deformation of metallic tubes with different cross-section areas such as a circular, square, triangle, or oblong. However, the crush behavior and collapse mechanism of circular-shaped tubes are the most investigated ones. In addition to the experimental studies, some other studies are focused on developing a theoretical model of circular tubes under lateral loading. As shown in Fig. 5 deformation of a circular tube under lateral loading was generated four stationary plastic hinges of which two are placed vertical and the others are placed horizontally. Under lateral loading, the vertical hinges are getting closer to each other while the horizontal ones are moving away from each other. According to the studies it is possible to say that increase in thickness and the decrease in the diameter enhance the mean crush load and the absorbed energy [13].

The force–displacement curve of the ST-3 tube, which is forced to be crushed radially between two rigid plates, is given in Fig. 5. The curve can be divided into two main parts in terms of the deformation behavior of the tube. These; i) the plateau region where the tube is deformed under almost constant load, and the tube diameter decreases in the direction of the force and ii) the full compression region where the force increases rapidly. In the plateau region, the tube cross-section transforms from circular to elliptical under the effect of force. At this stage, while points 1 & 2 on the sides move away from each other, points 3 & 4 get closer to each other. After the stage where the plateau region ends in the force–displacement curve, the 3 & 4 points that initially touch the rigid plates are directed towards the inside of the tube. This is especially the case with tubes with low yield strength. In the case of continued loading, when the distance between the upper and lower surfaces falls below a certain value, a full compression situation and a sudden increase in the force value occurs.

In Fig. 6., force–displacement curves of single steel tubes with the same wall thickness and different diameters are given under lateral load. In tubes with approximately the same strength, it is seen that the tube diameter has a dominant effect on the force curve. It is seen that the initial and plateau strength values increase with decreasing diameter, in accordance with the literature [27]. It is seen that the force values at the beginning and end of the plateau region remained approximately the same in the ST-1 sample, and this increased with decreasing diameter. This is because the moment force required for deformation with a smaller diameter is higher than for large diameter specimens [33]. Accordingly, the highest specific energy absorption was obtained in the ST-4 sample even it does not have the highest absorbed energy. The absorbed energy and the specific energy absorption (SEA) values of these samples are given in Table 3.

3.2. Lateral loading results of nested tube

Fig. 7. denotes the force–displacement curve in lateral crushing of the NT2 sample obtained by placing the ST-2 tube into the ST-1 tube. In the experiment, it was observed that the deformation started from the upper part of the ST-1 tube as expected, and the force proceeded similarly to the ST-1 tube. However, as can be seen in the figure, with a displacement of 40 mm, the ST-1 tube contacts the ST-2 tube, which has not been deformed yet, and these two tubes are deformed together in the ongoing process. At this point, the ST-2 tube also joined the deformation, increasing the force curve similar to the beginning of the experiment. This situation enabled the force curve to have a stepped characteristic.

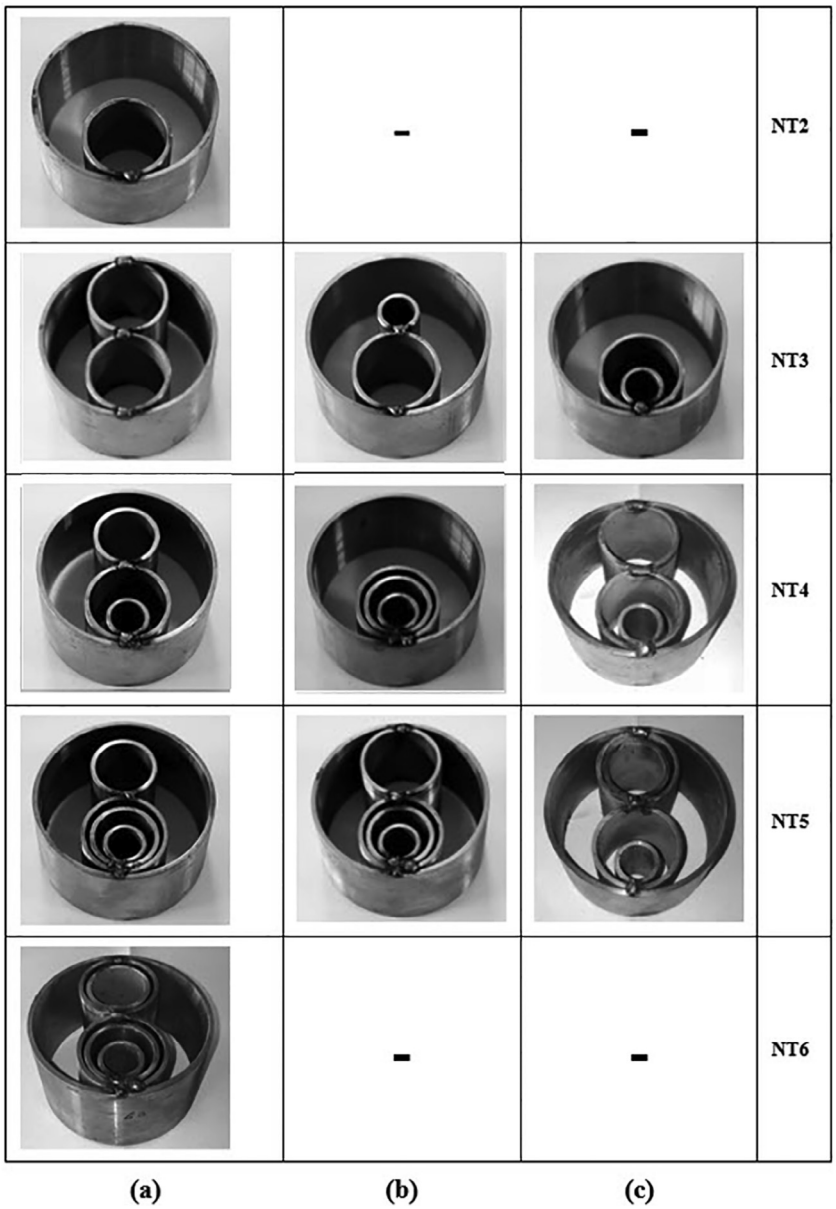

Fig. 3. Experimented nested tube configurations.

Table 2
The numbers of ST-1/4 tubes in nested tubes and the weight of nested tubes.

Sample name	Numbers of Tube Types				Weight (g)
	ST-1	ST-2	ST-3	ST-4	
NT2	1	1	0	0	313
NT3-A	1	2	0	0	411
NT3-B	1	1	0	1	355
NT3-C	1	1	0	1	355
NT4-A	1	1	1	1	435
NT4-B	1	1	1	1	435
NT4-C	1	2	0	1	454
NT5-A	1	1	2	1	515
NT5-B	1	2	1	1	533
NT5-C	1	2	1	1	533
NT6	1	2	2	1	613

Fig. 8. denotes the force–displacement curves of NT3 nested samples under lateral load. Since two ST-2 tubes are used in the NT3-A sample, these tubes are in contact with the ST-1 tube. In NT3-B and NT3-C samples, ST-2 and ST-4 tubes were used by changing their places. When the curves are examined, due to the contact of the tubes in the NT3-A sample, the deformation started

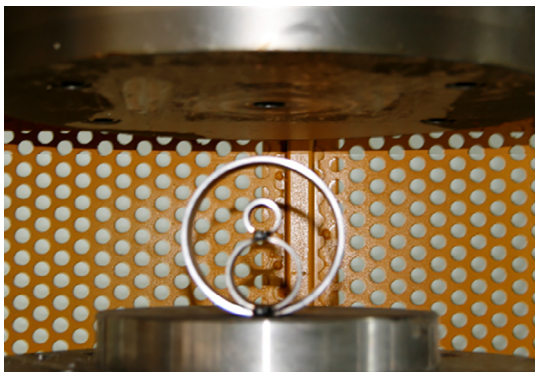

Fig. 4. Nested tubes prior to lateral loading.

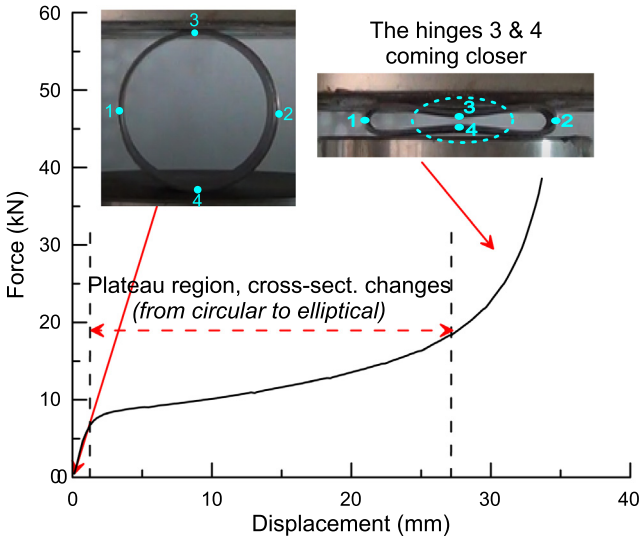

Fig. 5. The force–displacement curve of the ST-3 tube under lateral loading.

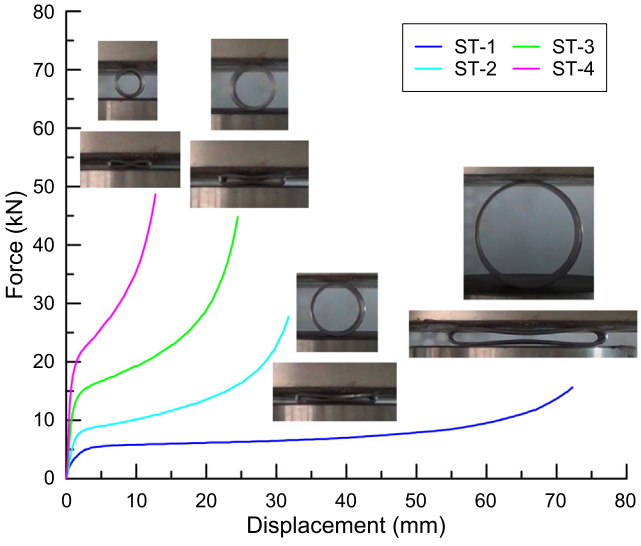

Fig. 6. The force–displacement curves of the ST tubes under lateral loading.

and progressed simultaneously in all tubes. As a result of this expected situation, a uniform curve was formed in contrast to the stepped curve in the NT2 sample in force. On the other hand,

Table 3
The absorbed energy and the specific energy absorption (SEA) values for ST-1 – ST-4 tubes.

Sample Name	Absorbed Energy (J)	Specific Energy Absorption (J/g)
ST-1	544	2.54
ST-2	413	4.21
ST-3	516	6.48
ST-4	364	8.48

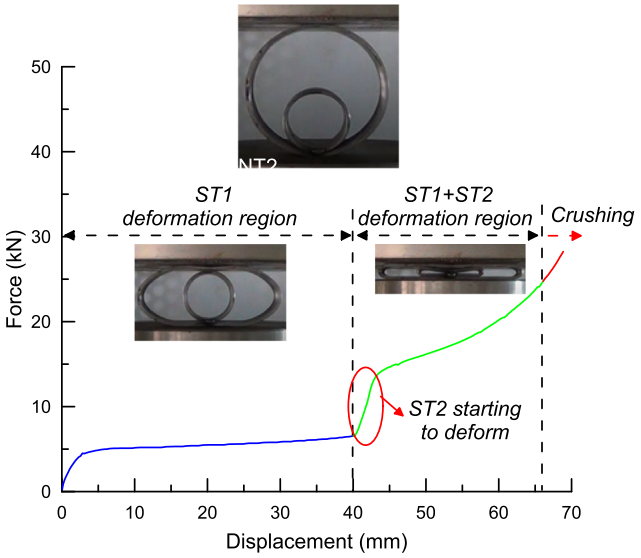

Fig. 7. The force–displacement curve of the NT2 sample under lateral loading.

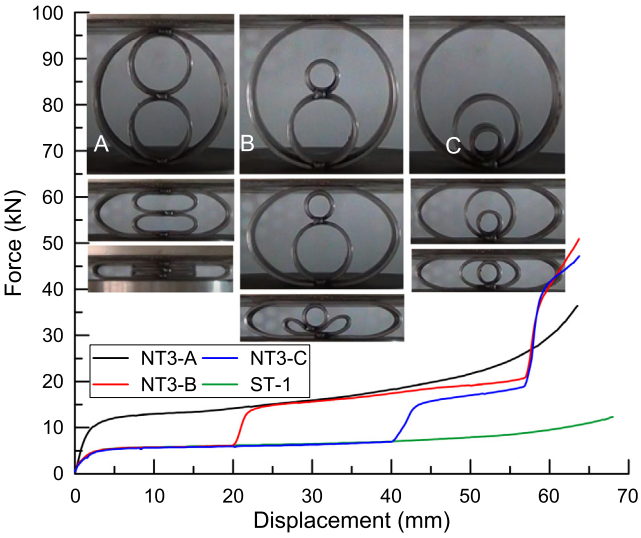

Fig. 8. The force–displacement curves of the NT3 group samples under lateral loading.

since the three tubes in the NT3-B and NT3-C samples are deformed independently and sequentially, a three-step curve was obtained similar to Fig. 7. This stepped situation in the force curve appears to be a crucial issue in terms of allowing the force to be increased at the desired rate at the desired displacement. At this point, the reason why the deformation continues in the ST-2 tube instead of the ST-4 tube in these two samples after the ST-1 tube is mentioned above. Therefore, it should be taken into account that

deformation will continue from large diameter tubes to small diameter tubes in nested tube combinations.

In Fig. 9., the energy-displacement curves of NT3 samples are given. In the figure, it is seen that the energy curve consists of three different regions with different slopes due to the stepped structure in the force curves of the NT3-B and NT3-C samples. In the NT3-A sample, it is possible to say that the curve exhibits an approximately linear increase, as the tubes are deformed together. The NT3-C sample absorbed the least energy among the three samples. When this value is taken as reference, it is seen that the NT3-B sample using the same tubes reached this energy value approximately 5 mm earlier. Besides, as can be seen from the graph, it is understood that the NT3-A sample reached this energy value 15 mm earlier and absorbed 1126 J energy, approximately 47% more than the NT3-C sample.

Fig. 10. denotes the force–displacement curves of NT4 sample combinations, and Fig. 11. denotes the energy-displacement curves of these samples. All single tubes were used to create samples in this group. In samples other than NT4-C, it is seen that the tubes are not in full contact with each other. In the NT4-B sample, because the outer tube first came into contact with the inner tubes after about 40 mm, the force curve was in the curved character of the ST-1 tube for 40 mm. This situation was reflected in the energy values given in Fig. 11. In addition, the energy curve showed a low increasing trend up to 40 mm displacement value. As a result, the lowest energy in this group was obtained as 893 J in this sample. The fact that the tubes in the NT4-C sample were in contact with the ST-1 tube caused the force curve to be higher initially. However, after approximately 25 mm of displacement value, the ST-3 tube in the NT4-A sample participated in the deformation and thus the force value of the sample was higher. When the energy curves are given in Fig. 11. are examined, it is seen that the NT4-C sample has a higher energy value up to 40 mm displacement, but the increase in the curve of the NT4-A sample is higher after 25 mm displacement. Moreover, this sample absorbed 53% higher energy than the NT4-B sample. This situation is very important in terms of showing the positive effect of the gradual increase in force on the absorbed energy value with an accurate design. Finally, the energy value of 750 J, referenced in Fig. 9., was obtained at 45 mm displacement value, which is approximately 5 mm lower than the NT3-A sample in the NT4-A sample.

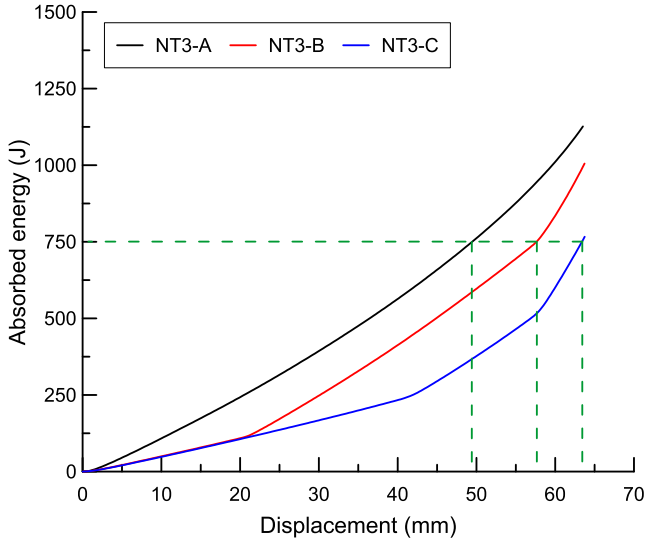

Fig. 9. The energy-displacement curves of the NT3 group samples under lateral loading.

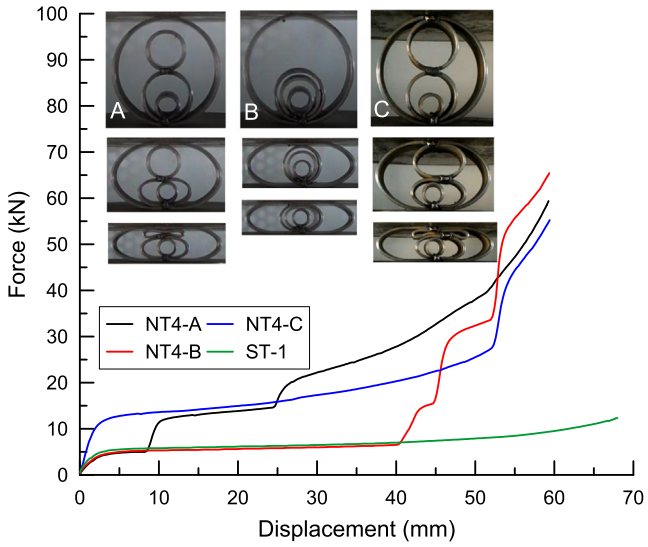

Fig. 10. The force–displacement curves of the NT4 group samples under lateral loading.

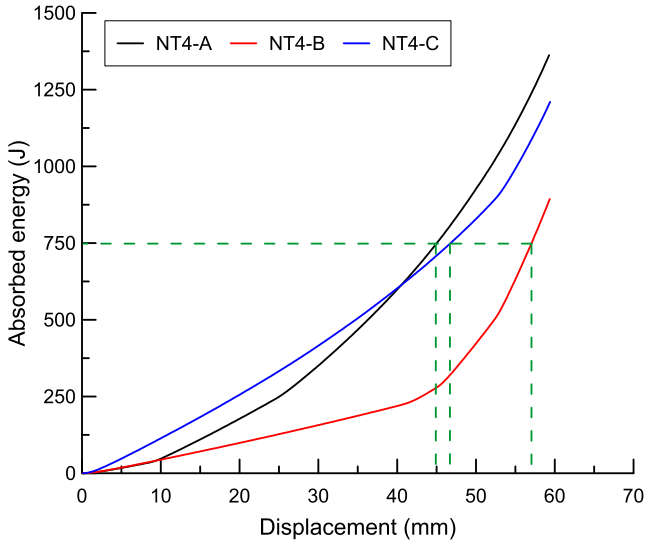

Fig. 11. The energy-displacement curves of the NT4 group samples under lateral loading.

In Fig. 12. and Fig. 13., force–displacement and energy-displacement curves of NT5 sample combinations are given, respectively. In these samples, the tubes are in contact with the NT5-B/C samples. Therefore, the initial forces of these two samples are higher than the NT5-A sample as seen in Fig. 12. Although the same tubes were used, the ST-3 and ST-4 tubes were placed in the ST-2 tube in the NT5-C sample, unlike the NT5-B sample. It is seen that this change caused the NT5-C sample, one of the samples with the same strength, to form another step that increases the force value at approximately 20 mm displacement (Fig. 12.). This situation is also evident in the energy curves given in Fig. 13. It is seen that the curve of the NT5-A sample, which has the lowest energy curve slope at the beginning, is above the energy curve of this sample due to the tube placement in the NT5-B sample with a displacement of approximately 25 mm. When Fig. 13. is examined, it is seen that there is an approximately 10 mm difference between the displacement values reaching 750 J in NT5-C/B samples created with different alignments of the same tubes.

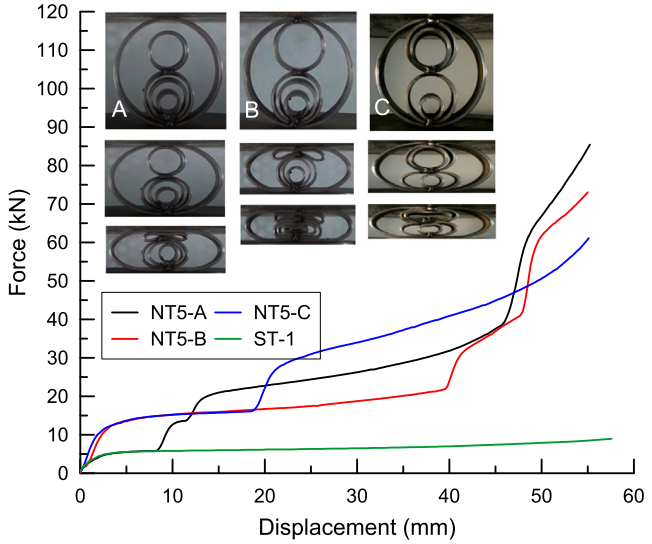

Fig. 12. The force–displacement curves of the NT5 group samples under lateral loading.

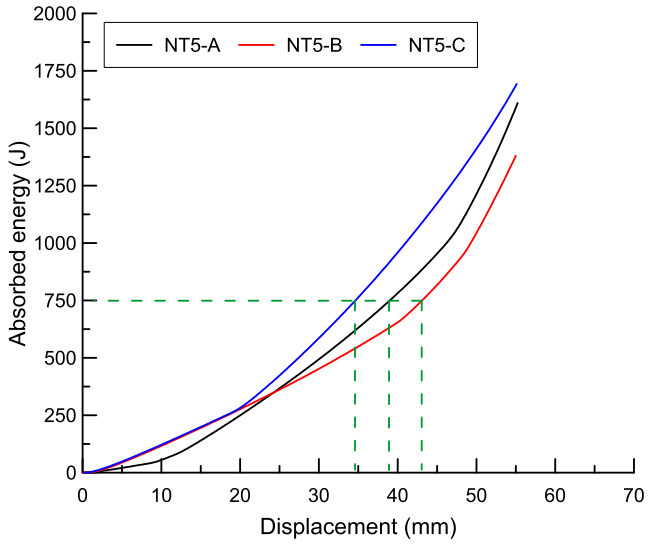

Fig. 13. The energy-displacement curves of the NT5 group samples under lateral loading.

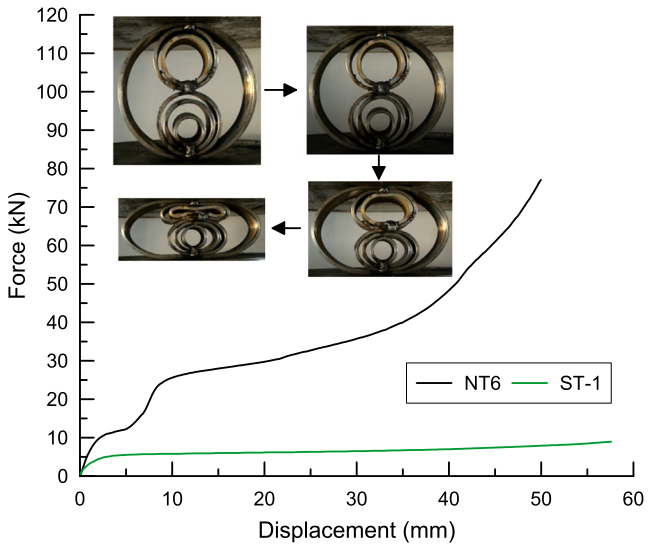

Fig. 14. The force–displacement curve of the NT6 sample under lateral loading.

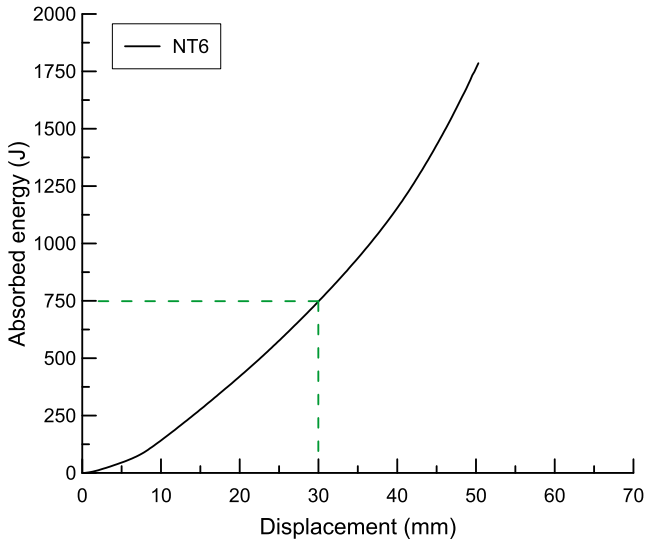

Fig. 15. The energy-displacement curve of the NT6 sample under lateral loading.

Fig. 14. denotes the force–displacement curve of the NT6 sample in which 5 tubes are used inside. The sample was created by placing two ST-2 and ST-3 tubes and one ST-4 tube into the ST-1 tube. It appears that the onset of force is similar to samples with the tubes in contact. In addition, as a result of the ST-3 tubes participating in the deformation with a displacement of about 6 mm, a second step in the force value was formed. When the energy-displacement curve given in Fig. 15. is examined, it is seen that the 750 J energy value in Fig. 9. is absorbed in 30 mm in this sample. The total energy absorbed is 1767 J. This value is approximately 29% and 5% higher than the lowest and highest energy values in the NT5 group, respectively. It should be noted that the number of tubes used in this sample affects the crushing displacement of the sample. The crush displacement value, which was 65 mm in the NT3 group, cannot even reach the 55 mm displacement value in the NT6 sample.

In Fig. 16., the force–displacement curves of the samples with the highest energy in each group are given together. In the NT4 sample only, the inner tubes encounter the outer tube. Therefore, the initial strength values of the other three samples are approximately the same as each other and approximately twice as high as the NT4 sample. The fact that there is a stepped structure arising from the design in the force values is also a remarkable issue. The first of the secondary increases in the force curves occurred in the NT6 sample at 6 mm displacement. It is seen that the crushing displacement value mentioned above is approximately 10 mm lower in the NT6 sample than in the NT4 sample. It is seen that the curve of the NT4 sample, although it was lower at the beginning, rose above the NT3 sample with the step effect at 25 mm displacement. This situation is very critical in terms of revealing how important the design is in such samples.

The energy-displacement curves of the samples given above are given in Fig. 17. It is seen that the energy values increased faster in the NT6 sample than in the others. This situation can be interpreted as the result of the efficient gradual increase in the force curve of the NT6 sample. Taking the maximum absorbed energy values into account, the one for the NT6 sample is approximately 57%, 30%, and 5% higher than that for NT3, NT4, and NT5 samples,

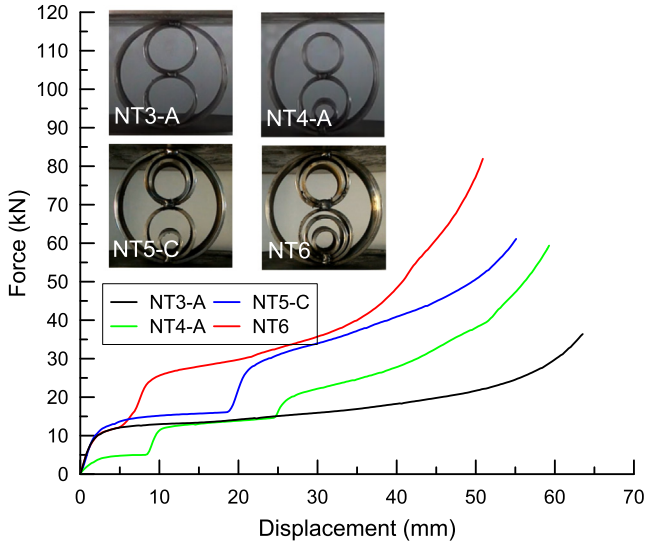

Fig. 16. The force–displacement curves of the NT3-A, NT4-A, NT5-C, and NT6 samples under lateral loading.

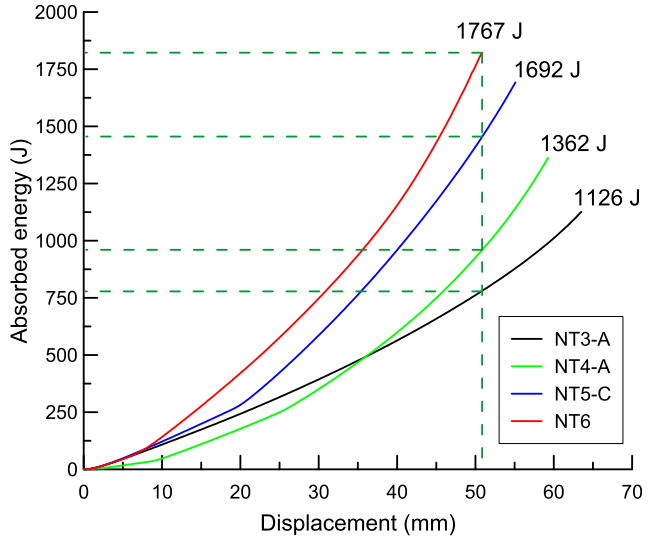

Fig. 17. The energy-displacement curves of the NT3-A, NT4-A, NT5-C, and NT6 samples.

respectively. Besides, if the energy values are recalculated for the same displacement, the energy absorbed by the NT6 sample is approximately 132% higher than the NT3 sample, which has the lowest energy and approximately 22% higher than the NT5 sample.

3.3. Energy absorption characteristic

As it is known, the main priority for energy-absorbing structures is to have absorbed energy as high as possible. In this context, the use of reinforcement elements or strength increasing methods to maximize energy value is a common situation in studies. However, it is essential that the energy absorbed is not only high but also efficient. Therefore, if there is a decrease in energy efficiency when using a method that provides energy increase in the tube structure, this method should not be preferred.

Yella [26] determined some criteria for an efficient energy-absorbing structure in their studies on the energy efficiency of tubular structures. One of these criteria is the ability to absorb specific energy (SEA). This parameter, whose numerical expression is given in Equation (1), is defined as the absorbed energy per unit weight.

$$SEA = \frac{E}{m} \tag{1}$$

Where m is the total mass of the energy-absorbing structure, and E is the total energy absorbed. The absorbed energy (E) corresponds to the area under the force–displacement curve of the structure. It can be calculated with the integral given in Equation (2).

$$E = \int_0^{\delta} F(\delta).d\delta \tag{2}$$

In Table 4, the absorbed energy, total weight, and the calculated SEA values of the nested tube samples used in the experimental study are given together. It is not overlooked that the NT3-A sample, which absorbs the highest energy in the NT3 group, is not the most efficient in its group in terms of SEA value. Besides, it is seen that the lowest and highest energy absorbed was obtained in NT2 and NT6 samples, respectively. However, considering the sample weights, the highest and lowest SEA values were obtained in NT4-B and NT5-C samples, respectively. Therefore, it is concluded that the NT4-B sample, which absorbs approximately 26% higher energy than the NT2 sample, is not an efficient design. Similarly, it is possible to say that the NT5-C sample, which absorbs 5% less energy than the NT6 sample, is more efficient than this sample in terms of design.

The SEA values of the samples with the highest energy in each group are shown together in the bar graph given in Fig. 18. The SEA value of the NT5-C sample is about 16% higher than the NT3-A sample. While the NT6 sample was 5% higher than the NT5-C sample in terms of absorbed energy, the SEA value was calculated to be 10% lower (Fig. 18.). It can be said that this is since the NT6 sample contains one more ST-3 tube than the NT5-C sample in the design. Moreover, while the NT4-A sample absorbed 24% less energy, it was almost (difference in SEA values is ~ 1%) equal to the NT5-C sample in terms of SEA value.

In order to determine the most efficient design, in addition to the SEA parameter, the work effectiveness (W_{eff}) given in Equation (3) and the energy efficiency (e_E) parameters given in Equation (4) was also taken into consideration.

$$W_{eff} = SEA \times e_g \tag{3}$$

$$e_E = \frac{E}{F_{max} \times \delta} \tag{4}$$

e_g seen in Equation (3) denotes the crush displacement efficiency and it is calculated as the ratio of the displacement value at which the sample can be crushed to the original diameter of the sample. In Equation (4), E is the absorbed energy value, Fmax

Table 4
SEA values for nested tube samples.

Specimens Nested tube, (NT)	Weight (g)	Energy (J)	SEA (J/g)
NT2	313	709	2.26
NT3-A	411	1126	2.74
NT3-B	356	1005	2.83
NT3-C	356	766	2.15
NT4-A	435	1362	3.13
NT4-B	435	893	2.05
NT4-C	454	1210	2.67
NT5-A	515	1610	3.13
NT5-B	533	1380	2.59
NT5-C	533	1692	3.17
NT6	613	1767	2.88

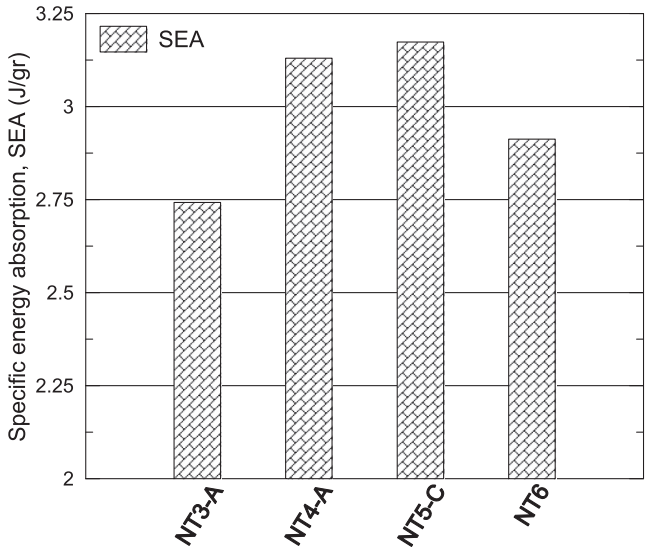

Fig. 18. SEA values for the NT4-A, NT5-C, and NT6 samples.

is the highest force value on the force–displacement curve, and δ is the final crush displacement value of the sample. Here, according to the parameter given in Equation (4), it would be appropriate to say that energy-absorbing structures with force–displacement curves in a form close to rectangular will have very high efficiency in terms of energy efficiency.

In Fig. 19., W_{eff} and e_E values calculated for NT4-A, NT5-C, and NT6 samples are given together in the bar graph. At this stage, the NT3-A sample, which had a low performance in terms of SEA and absorbed much lower energy than the other samples, was not taken into account, the evaluation was made between NT4-A, NT5-C, and NT6 samples. It is clear from the graph that the sample exhibiting the most efficient properties for both parameters is NT5-C. The sample has a value of 50% in terms of energy efficiency. The closest ratio to this value is 43% in the NT6 sample. While there is a clear difference with the NT4-A sample in the work effectiveness values, this difference is quite small with the NT6 sample.

As a result, the NT5-C sample is more efficient design in terms of SEA, W_{eff} and e_E than other nested tubes. Besides, the fact that the energy absorbed by this sample is very close to the NT6 sample, which absorbs the highest energy, indicates that it can be preferred for an energy-absorbing structure. If higher energy values are required, the energy absorption capacity of the sample can be increased by *i)* increasing the displacement values by using tubes with larger diameters and *ii)* shifting the force values upwards by using wider tubes with the same tube diameters.

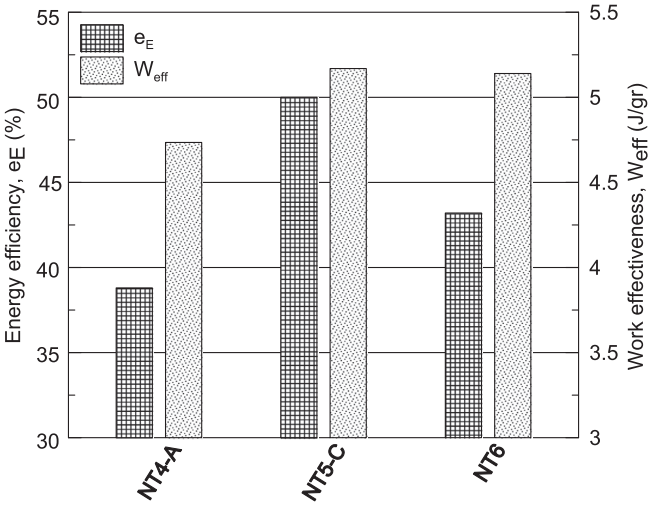

Fig. 19. Work effectiveness (W_{eff}) and energy efficiency (e_E) values for the NT4-A, NT5-C, and NT6 samples.

4. Conclusion

In this study, the deformation behavior of steel tubes under lateral load and their energy absorption ability was investigated. In addition to single steel tubes, nested tubes in different combinations made from these tubes were also used in experimental studies. In single tubes, the highest energy was found in the tube with the biggest diameter (ST-1) however, the highest force value occurred in the tube with the lowest diameter (ST-4). This increase in the force value is because the moment to initiate the deformation in the tube is higher with the smaller diameter. The highest energy value was obtained as 1767 J in the nested tube sample that contains 6 tubes (NT6), although it had the lowest crush displacement value. In the determination of the most efficient design, specific energy absorption ability, work effectiveness, and energy efficiency parameters were taken into consideration as well as the absorbed energy. As a result, the 5 tubes used nested tube configuration (NT5-C), which offers higher values in all three parameters than all other samples, has come to the fore as the most efficient design, although it does not absorb the highest energy. If higher energy values in the same geometric dimensions are required, higher strength tubes can be used. In cases where the change in geometric dimensions is insignificant, the crush displacement value can be increased by using larger diameter tubes. Besides, the desired value can be reached by shifting the force values upwards, depending on the increase in tube widths.

Declaration of Competing Interest

The authors declare that they have no known competing financial interests or personal relationships that could have appeared to influence the work reported in this paper.

References

[1] M.A. Guler, M.E. Cerit, B. Bayram, B. Gerçeker, E. Karakaya, The effect of geometrical parameters on the energy absorption characteristics of thin-walled structures under axial impact loading, Int. J. Crashworthiness 15 (4) (2010) 377–390, https://doi.org/10.1080/13588260903488750.
[2] S. Pirmohammad, S.E. Marzdashti, Crushing behavior of new designed multi-cell members subjected to axial and oblique quasi-static loads, Thin-Walled Struct. 108 (2016) 291–304, https://doi.org/10.1016/j.tws.2016.08.023.
[3] Q. Gao, L. Wang, Y. Wang, C. Wang, Crushing analysis and multiobjective crashworthiness optimization of foam-filled ellipse tubes under oblique impact loading, Thin-Walled Struct. 100 (2016) 105–112, https://doi.org/10.1016/j.tws.2015.11.020.
[4] B. Simhachalam, K. Srinivas, C.L. Rao, Energy absorption characteristics of aluminium alloy AA7XXX and AA6061 tubes subjected to static and dynamic axial load, 8265 (2014). doi:10.1080/13588265.2013.878974.
[5] W. Abramowicz, N. Jones, Dynamic progressive buckling of circular and square tubes, Int. J. Impact Eng. 4 (4) (1986) 243–270, https://doi.org/10.1016/0734-743X(86)90017-5.
[6] M.M. Yalçın, K. Genel, On the axial crush performance of PVC foam-filled aluminum/CFRP hybrid circular tube, Sakarya Univ. J. Sci. 23 (2019) 1154–1162, https://doi.org/10.16984/saufenbilder.581542.
[7] Ø. Jensen, M. Langseth, O.S. Hopperstad, Hopperstad, Experimental investigations on the behaviour of short to long square aluminium tubes subjected to axial loading, Int. J. Impact Eng. 30 (8-9) (2004) 973–1003, https://doi.org/10.1016/j.ijimpeng.2004.05.002.
[8] M.M. Yalçın, K. Genel, On the axial deformation characteristic of PVC foam-filled circular aluminium tube: Effect of radially-graded foam filling, Thin-Walled Struct. 144 (2019) 106335, https://doi.org/10.1016/j.tws.2019.106335.
[9] O.H. Mete, M. Yalcin, K. Genel, Experimental and numerical studies on the folding response of annular-rolled Al tube, Thin-Walled Struct. 127 (2018) 798–808, https://doi.org/10.1016/j.tws.2018.03.015.
[10] V.S. Deshpande, N.A. Fleck, High strain rate compressive behaviour of aluminum alloy foams, Int. J. Impact Eng. 24 (2000) 277–298, https://doi.org/10.1016/S0734-743X(99)00153-0.

[11] A.G. Hanssen, M. Langseth, O.S. Hopperstad, Static and dynamic crushing of circular aluminium extrusions with aluminium foam filler, Int. J. Impact Eng. 24 (5) (2000) 475–507, https://doi.org/10.1016/S0734-743X(99)00170-0.
[12] Q. Gao, L. Wang, Y. Wang, C. Wang, Multi-objective optimization of a tapered elliptical tube under oblique impact loading, Proceed. Instit. Mech. Eng. Part D: J. Auto. Eng. 231 (14) (2017) 1978–1988, https://doi.org/10.1177/0954407017690963.
[13] A. Baroutaji, M.D. Gilchrist, D. Smyth, A.G. Olabi, Crush analysis and multi-objective optimization design for circular tube under quasi-static lateral loading, Thin-Walled Struct. 86 (2015) 121–131, https://doi.org/10.1016/j.tws.2014.08.018.
[14] E. Morris, A.G. Olabi, M.S.J. Hashmi, Analysis of nested tube type energy absorbers with different indenters and exterior constraints, Thin-Walled Struct. 44 (8) (2006) 872–885, https://doi.org/10.1016/j.tws.2006.08.014.
[15] H. Wang, J. Yang, H. Liu, Y. Sun, T.X. Yu, Internally nested circular tube system subjected to lateral impact loading, Thin-Walled Struct. 91 (2015) 72–81, https://doi.org/10.1016/j.tws.2015.02.014.
[16] T.N. Tran, A study on nested two-tube structures subjected to lateral crushing, Thin-Walled Struct. 129 (2018) 418–428, https://doi.org/10.1016/j.tws.2018.04.022.
[17] B. Xu, C. Wang, W. Xu, An efficient energy absorber based on fourfold-tube nested circular tube system, Thin-Walled Struct. 137 (2019) 143–150, https://doi.org/10.1016/j.tws.2019.01.026.
[18] L. Wu, J.F. Carney, Experimental analyses of collapse behaviors of braced elliptical tubes under lateral compression, Int. J. Mech. Sci. 40 (8) (1998) 761–777, https://doi.org/10.1016/S0020-7403(97)00121-5.
[19] T.N. Tran, T.N.T. Ton, Lateral crushing behaviour and theoretical prediction of thin-walled rectangular and square tubes, Compos. Struct. 154 (2016) 374–384, https://doi.org/10.1016/j.compstruct.2016.07.068.
[20] A.G. Hanssen, O.S. Hopperstad, M. Langseth, Design of aluminium foam-filled crash boxes of square and circular cross-sections, Int. J. Crashworthiness 6 (2) (2001) 177–188, https://doi.org/10.1533/cras.2001.0171.
[21] S.C.K. Yuen, G.N. Nurick, The energy-absorbing characteristics of tubular structures with geometric and material modifications : An overview, Appl. Mech. Rev. ASME. 61 (2008) 1–15, https://doi.org/10.1115/1.2885138.
[22] M.M. Yalçın, O.H. Mete, K. Genel, Axial crushing behavior of circular aluminum tubes, Mater. Test.. 61 (8) (2019) 749–754, https://doi.org/10.3139/120.111380.
[23] A. Baroutaji, M.D. Gilchrist, A.G. Olabi, Quasi-static, impact and energy absorption of internally nested tubes subjected to lateral loading, Thin Walled Struct. 98 (2016) 337–350, https://doi.org/10.1016/j.tws.2015.10.001.
[24] T.Y. Reddy, S.R. Reid, Phenomena associated with the crushing of metal tubes between rigid plates, Int. J. Solids Struct. 16 (6) (1980) 545–562, https://doi.org/10.1016/0020-7683(80)90005-0.
[25] J.A. DeRuntz P.G. Hodge Crushing of a Tube Between Rigid Plates 30 3 1963 391 395 10.1115/1.3636567
[26] T. Yella Reddy, S.R. Reid, Lateral compression of tubes and tube-systems with side constraints, Int. J. Mech. Sci. 21 (3) (1979) 187–199, https://doi.org/10.1016/0020-7403(79)90023-7.
[27] N.K. Gupta, G.S. Sekhon, P.K. Gupta, A study of lateral collapse of square and rectangular metallic tubes, Thin-Walled Struct. 39 (9) (2001) 745–772, https://doi.org/10.1016/S0263-8231(01)00033-7.
[28] S. Sinaie, T.D. Ngo, V.P. Nguyen, T. Rabczuk, Validation of the material point method for the simulation of thin-walled tubes under lateral compression, Thin-Walled Struct. 130 (2018) 32–46, https://doi.org/10.1016/j.tws.2018.05.014.
[29] A.A.A. Alghamdi, Collapsible impact energy absorbers: an overview, Thin-Walled Struct. 39 (2) (2001) 189–213, https://doi.org/10.1016/S0263-8231(00)00048-3.
[30] E. Linul, N. Movahedi, L. Marsavina, On the lateral compressive behavior of empty and ex-situ aluminum foam-filled tubes at high temperature, Materials. 11 (4) (2018) 554, https://doi.org/10.3390/ma11040554.
[31] B. Zhang, L.i. Wang, J. Zhang, Y. Jiang, W. Wang, G. Wu, Deformation and energy absorption properties of cenosphere/aluminum syntactic foam-filled circular tubes under lateral quasi-static compression, Int. J. Mech. Sci. 192 (2021) 106126, https://doi.org/10.1016/j.ijmecsci.2020.106126.
[32] A.G. Olabi, E. Morris, M.S.J. Hashmi, M.D. Gilchrist, Optimised design of nested circular tube energy absorbers under lateral impact loading, Int. J. Mech. Sci. 50 (1) (2008) 104–116, https://doi.org/10.1016/j.ijmecsci.2007.04.005.
[33] A.G. Olabi, E. Morris, M.S.J. Hashmi, M.D. Gilchrist, Optimised design of nested oblong tube energy absorbers under lateral impact loading, Int. J. Impact Eng. 35 (1) (2008) 10–26, https://doi.org/10.1016/j.ijimpeng.2006.11.007.
[34] Z.L. Yu, P. Xue, Z. Chen, Nested tube system applicable to protective structures against blast shock, Int. J. Impact Eng. 102 (2017) 129–139, https://doi.org/10.1016/j.ijimpeng.2016.11.018.